Materials Research Proceedings 41 (2024) 1925-1934 https://doi.org/10.21741/9781644903131-213

Influence of the depth of cut on the AM nitinol properties in flood and cryogenic machining

GUARISE Alessandra[1,a], BERTOLINI Rachele[1,b], GHIOTTI Andrea[1,c], BRUSCHI Stefania[1,d*]

[1]Department of Industrial Engineering (DII), University of Padova, Via Venezia 1, 35131, Padova, Italy

[a]alessandra.guarise@phd.unipd.it, [b]rachele.bertolini@unipd.it, [c]andrea.ghiotti@unipd.it, [d]stefania.bruschi@unipd.it

Keywords: Nitinol, Additive Manufacturing, Machining, Depth of Cut, Surface Finish

Abstract. Nickel-titanium alloys, commonly called Nitinol, are known for two fundamental properties, namely the shape memory effect (SME) and the superelasticity effect (SE), which make Nitinol a material of great interest for applications in various fields, such as biomedical, aerospace, automotive, and electronics. Most of the published research studies discuss the Nitinol properties after just one step of fabrication, e.g. forming, casting, additive manufacturing (AM), or machining. On the contrary, this work focuses on a process chain including AM followed by heat treatment and both flood and cryogenic machining. In particular, the depth of cut during the last machining step was varied (0.1, 0.25, and 0.4 mm), to investigate its effects on the AM and heat-treated Nitinol in terms of machined surface finish and transformation temperatures. It was found that when cutting with a depth of cut of 0.25 mm, the workpiece shows the worst roughness, regardless of the material microstructure and machining condition. However, for other depths of cut, there is a clear improvement in terms of surface finish. Machining increases the Nitinol transformation temperatures, but changing the depth of cut does not have a significant effect. Cryogenic machining induces a worse surface finish, but has less effect on the transformation temperatures than flood machining.

Introduction

Nitinol (hereafter called NiTi) alloy is a type of shape memory alloy (SMA) and is commonly known as 'metal with a memory'. It was discovered in 1959 at the U.S. Naval Ordnance Laboratory and is named Nitinol after its composition of nickel and titanium and the initials of the laboratory [1]. Because of its unique characteristics, this material is considered revolutionary for manufacturing engineering parts devoted to the biomedical and aerospace sectors. NiTi exhibits a martensitic transformation due to thermo-mechanical loads and recovers large inelastic strains upon unloading [2]. The martensitic transformation occurs when the crystal lattice changes from the high temperature high-symmetry austenitic parent phase to the low temperature, low-symmetry martensitic phase. Transformation can be achieved in two different ways, which correspond to the shape memory effect (SME) and superelasticity (SE). The shape memory effect happens when the material is cooled to a temperature below the martensite finish, causing the alloy to transform from the austenitic to the fully martensitic phase. If a mechanical load is applied at this point, the material undergoes large, microscopic inelastic strains. However, when heated to a temperature higher than the austenite finish, it returns to the austenitic phase, and the inelastic strains are recovered. The superelastic effect occurs when a load is applied to the material in the austenitic phase, inducing martensitic transformation. Upon release of the load, the reverse transformation occurs, resulting in the recovery of the load-induced strains.

The NiTi characteristics and properties are closely related to its actual chemical composition. NiTi parts obtained from additive manufacturing (AM) exhibit the shape memory effect when

fabricated from a Ti-rich powder, on the contrary, superelasticity effect is achieved when the parts are made from a Ni-rich powder [3].

Numerous studies have investigated the machinability of the wrought NiTi during finishing machining, investigating the effects of the cutting parameters on the NiTi properties. For instance, in [4] it was investigated the impact of the cutting speed on the surface integrity of hot-rolled Ni-rich NiTi samples during cryogenic and dry machining. The study revealed that cryogenic machining is more beneficial than dry cutting, and that the cutting speed has a strong influence on the surface and subsurface of the processed NiTi samples. Also in [5] it was studied the effect of the cutting speed on hot-forged Ni-rich NiTi dry machined samples, finding that, at low cutting speeds, there is a higher radial shape recovery of the machined material due to the phase transformations that are induced. To achieve this, in [5] it was analyzed the material phase and temperature distribution during the machining operation.

Previous research has also explored various techniques and process parameters for manufacturing NiTi components using AM, with the aim of achieving a "complexity for free" manufacturing process. However, if the goal is to obtain a final product, it is essential to combine AM with heat treatment and finishing processes and analyze the manufacturing impact at each stage on the final NiTi characteristics. In [6] AM NiTi specimens aged at 600°C and cryogenically machined were shown to exhibit superior surface integrity and superelasticity compared to both untreated specimens and those machined with conventional cutting fluids.

Nevertheless, there is still a lack of research that examines the entire process from AM to finishing machining at varying process parameters, especially the ones of the final machining step. To this aim, a Ni-rich NiTi alloy was used in a process chain that includes the fabrication of NiTi parts by AM, followed by heat treatments at various aging temperatures, and finally finishing machining using different depths of cut, both under flood and cryogenic cooling conditions. The effect of varying the depth of cut is evaluated by characterizing the machined material in terms of surface roughness, surface defects and transformation temperatures.

Materials and Methods

Laser powder bed fusion (LPBF) was used as first step of the process chain shown in Fig. 1 to fabricate NiTi cylinders of 40 mm height and 10 mm diameter, making use of the parameters reported in Table 1. The LPBF parameters were optimized in a previous work [7] to have NiTi samples with an austenitic microstructure at room temperature after AM. Pre-alloyed spherical Ni-rich $Ni_{50.4}Ti_{49.6}$ (at%) powders produced by gas atomization (ECKART TLS™) from an as-cast ingot in a size range between 15 μm and 45 μm were used for the LPBF process.

Table 1: LPBF optimized parameters [7].

Power [W]	Scanning speed [mm/s]	Hatch distance [mm]	Layer thickness [mm]	Oxygen level [ppm]
70	1100	0.06	0.025	<200

LPBF is usually followed by a heat treatment to relieve the residual stresses introduced by AM; in the case of Ni-rich NiTi, the post-AM heat treatment is also used to emphasize the material superelasticity thanks to the formation of Ni-rich precipitates through ageing [3]. The chosen heat treatment was carried out in a Carbolite Gero™ CWF 1200 furnace. Firstly, a relief annealing was performed at 1060°C for 60 minutes in an argon atmosphere, followed by rapid cooling in water. Subsequently, two sets of samples were aged at two different temperatures, namely 300°C (hereafter these samples are referred to as T3) and 600°C (hereafter these samples are referred to as T6). Both the ageing steps lasted 180 minutes and were followed by air cooling till room

temperature. For sake of comparison, another set of samples was considered, namely the as-built (AB) samples that did not undergo any heat treatment.

After AM, finishing machining is often mandatory to ensure the part's final geometry and properties. To this regard, the AB, T3 and T6 samples were turned at varying depth of cut on a Mori Seiki™ NL1500 CNC lathe using VCEX 110301L-F 1125 inserts. The cutting speed and feed were kept constant and equal to 31 m/min and 0.07 mm/rev, respectively. The turning trials were carried out using both a conventional cutting fluid and liquid nitrogen (LN_2). Details regarding the cryogenic apparatus mounted on the lathe can be found in [8]. Table 2 reports the finish machining parameters.

Table 2: Finishing machining parameters.

Lubricating-cooling conditions	Depth of cut a_p [mm]	Cutting speed V [m/min]	Feed f [mm/rev]	Length of turning L [mm]
Flood (F), Cryo (C)	0.1, 0.25, 0.4	31	0.07	3

The differences between the AB, T3 and T6 samples were first assessed by comparing the microstructures, which were observed using a Leica™ DMR light microscope. Cross-section pieces for microstructural analysis were cut from the NiTi cylinders using the Brillant 210A QATM™ cut off machine applying a coolant to prevent unwanted changes in the material due to temperature rise. The NiTi pieces were mounted in resin, polished with sandpaper, and then fine-polished in a solution containing 2/3 alkaline silica suspension and 1/3 volume of 30% hydrogen peroxide (H_2O_2). Finally, they were etched in a solution of HF (3.2 mL), HNO_3 (14.1 mL), and water (82.7 mL) for 45 seconds.

The knowledge of the NiTi transformation temperatures (TTs), defined as austenite start and finish (A_s, A_f), and martensite start and finish (M_s, M_f), is crucial for determining whether the material is in the austenitic (B2) or martensitic (B19') phase, or in the transformation zone (B2⇄B19'), at a given temperature, and therefore for assessing the impact of the process chain parameters on the NiTi superelasticity. The TTs were evaluated by means of differential scanning calorimetry (DSC) making use of the DSC Q200™ instrument, according to the F2004-17 standard [9]. For the DSC analysis, NiTi pieces of 30-50 mg were cut using the cut off machine, from both the center of the material (bulk) and the surface to assess the machining effects. The cycle that was adopted in the DSC analysis consists of cooling down to -70°C and heating the sample to 120°C at a heating-cooling rate of 10°C/min.

The surface of the machined samples was analysed using the Sensofar Plu Neox™ 3D optical profiler, which provides a 3D image of the sample's topography. The post-processing with the sensoVIEW™ software was carried out according to the ISO 25178 standard [10] which involves using a λ_s filter of 0.25 μm, a cut-off λ_c of 0.25 μm for an evaluation length of 1.25 mm.

Finally, the wear condition of the inserts and the state of the workpiece surface were examined using the FEI QUANTA 450™ scanning electron microscope (SEM) equipped with the secondary electron and backscattered detectors.

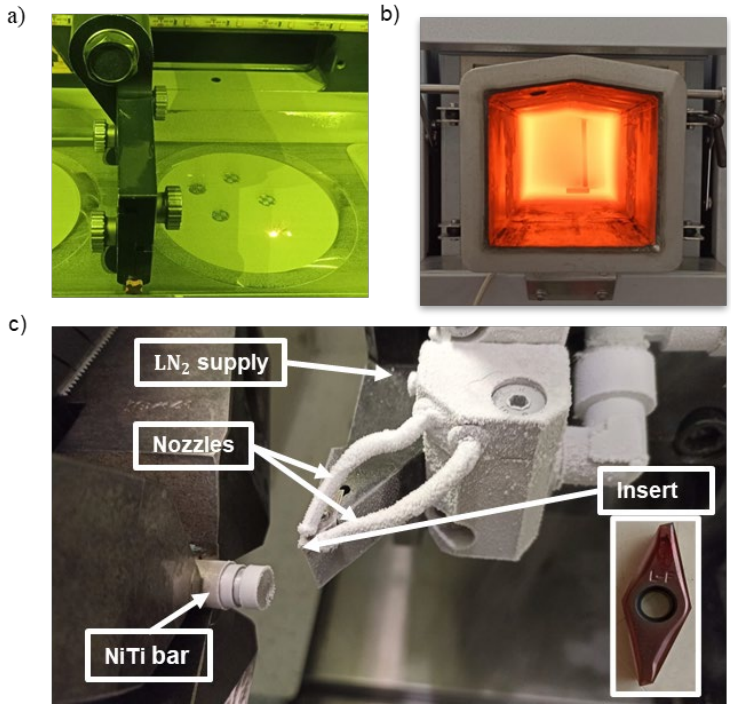

Fig. 1 Process chain for fabricating the NiTi samples: a) LPBF, b) heat treatment, and c) finishing machining (here shown with the cryogenic cooling apparatus).

Results and Discussion

Pre-machining Characteristics**.** Fig. 2 shows the microstructure of the AB, T3, and T6 samples obtained using the light microscope. The images depict a cross-section of the sample that is perpendicular to the building direction (BD). The microstructure is the primary factor distinguishing the samples that underwent different steps before machining. The AB sample exhibits a conventional post-AM microstructure, characterized by equiaxed grains with an average size equivalent to the hatch distance (60 µm). Upon heat treatment, the grain morphology of the AB sample is replaced by larger, irregularly shaped grains. This results in grain coarsening and the formation of various precipitates, whose chemical composition and morphology vary depending on the adopted ageing parameters.

Table 3 displays the martensite start and finish, as well as austenite start and finish values. When considering A_f, which sets the temperature at which the material can be considered austenitic, the two heat-treated samples behave differently when compared to the AB sample. The T3 sample shows an increase in A_f of 65.4%, while, on the contrary, the T6 sample shows a decrease of 30.8% compared to the AB one.

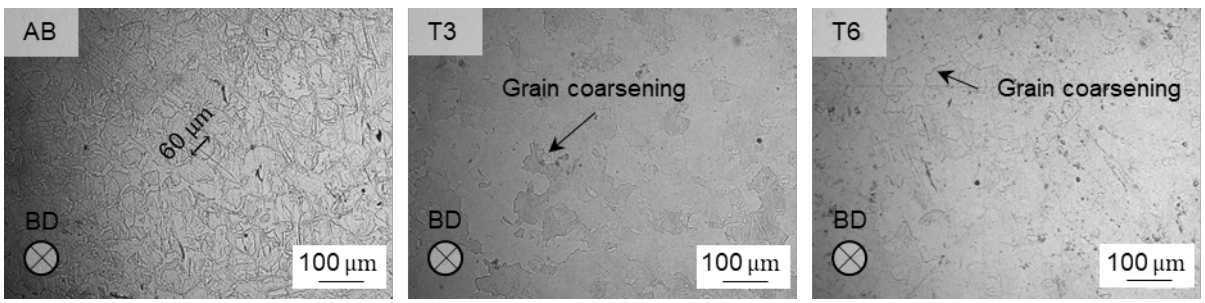

Fig. 2: Optical micrographs of the AB, T3 and T6 samples.

The different behaviour of the two heat treatments can be attributed to the types of precipitates formed because of ageing. Specifically, ageing the Ni-rich NiTi at approximately 300°C results in

the formation of small precipitates that induce an intermediate phase between austenite and martensite, known as the R-phase [11] . When aged at 600°C, different precipitates in terms of size and composition form compared to those at 300°C. The precipitates developed at 600°C promote the direct transformation between austenite and martensite, without the formation of the intermediate R-phase [6]. The presence of the R-phase results in higher transformation temperatures, which explains why the sample aged at 300°C has higher TTs than the other ones. Finally, Table 3 shows that, before machining, the material is always austenitic at room temperature regardless of its specific microstructure.

For completeness, here are reported the hardness values of the pre-machined samples according to a previous work by the authors [6], focusing on the same material and same microstructures as in this study, namely T6 was found to be the hardest sample (8.99 $\pm$ 1.24 GPa), followed by the AB sample (6.58 $\pm$ 1.38 GPa), and finally the T3 sample (3.43 $\pm$ 0.47 GPa).

Table 3: Transformation temperatures of the samples before machining.

	M_s [°C]	M_f [°C]	A_s [°C]	A_f [°C]
AB	-8 $\pm$ 2	-65$\pm$ 1	-18$\pm$ 3	13$\pm$ 0.5
T3	-5$\pm$ 4	-64$\pm$ 2	-6$\pm$ 2	21.5$\pm$ 1
T6	-17$\pm$ 3	-63$\pm$ 1	-15$\pm$ 1	9$\pm$ 2

Post-machining Characteristics. Fig. 3a displays the surface roughness S_a of the AB, T3, and T6 samples machined at varying depth of cut under flood and cryogenic cooling conditions. The results indicate that the depth of cut of 0.25 mm consistently produces the highest roughness value regardless of the material's microstructure and machining condition. In the flood case, the S_a values for the depths of cut at 0.1 and 0.4 mm are very similar between samples AB, T3 and T6. However, when cryogenic cooling is applied, the heat-treated samples machined at the maximum depth of cut have the lowest roughness, whereas the AB samples have the lowest roughness at $a_p$of 0.1 mm. In addition, the samples aged at 300°C show the best surface finish under both lubricating-cooling conditions and whatever the depth of cut. It is worth noting that the T3 samples are the least affected by the machining conditions.

When comparing flood and cryogenic machining, it is evident that the former induces a better surface in terms of S_a, particularly at a depth of cut of 0.25 mm. Differences are also noticeable at a_p of 0.1 mm, while at a_p of 0.4 mm, the S_a values of the flood machined samples are similar to those of the cryogenic machined ones. In the cryogenic case, the variation of S_a at varying depth of cut is greater than in the flood case. For instance, under cryogenic conditions, the AB sample machined at $a_p$of 0.4 mm shows a S_a 54% lower than the AB sample machined at $a_p$of 0.25 mm. In comparison, the same sample processed under flood conditions shows a 29% decrease in S_a between the same depths of cut. The reason for the observed differences between the two machining conditions can be ascribed to the material phase during cryogenic machining. The application of liquid nitrogen during machining reduces the cutting temperatures to a great extent. Therefore, it can be assumed that the material cryogenic machined at $a_p$of 0.25 mm is in the martensitic phase, i.e. at a temperature below M_s. However, as the depth of cut increases, the temperature also increases, and the NiTi is possibly machined in its austenitic phase or intermediate phase between martensite and austenite.

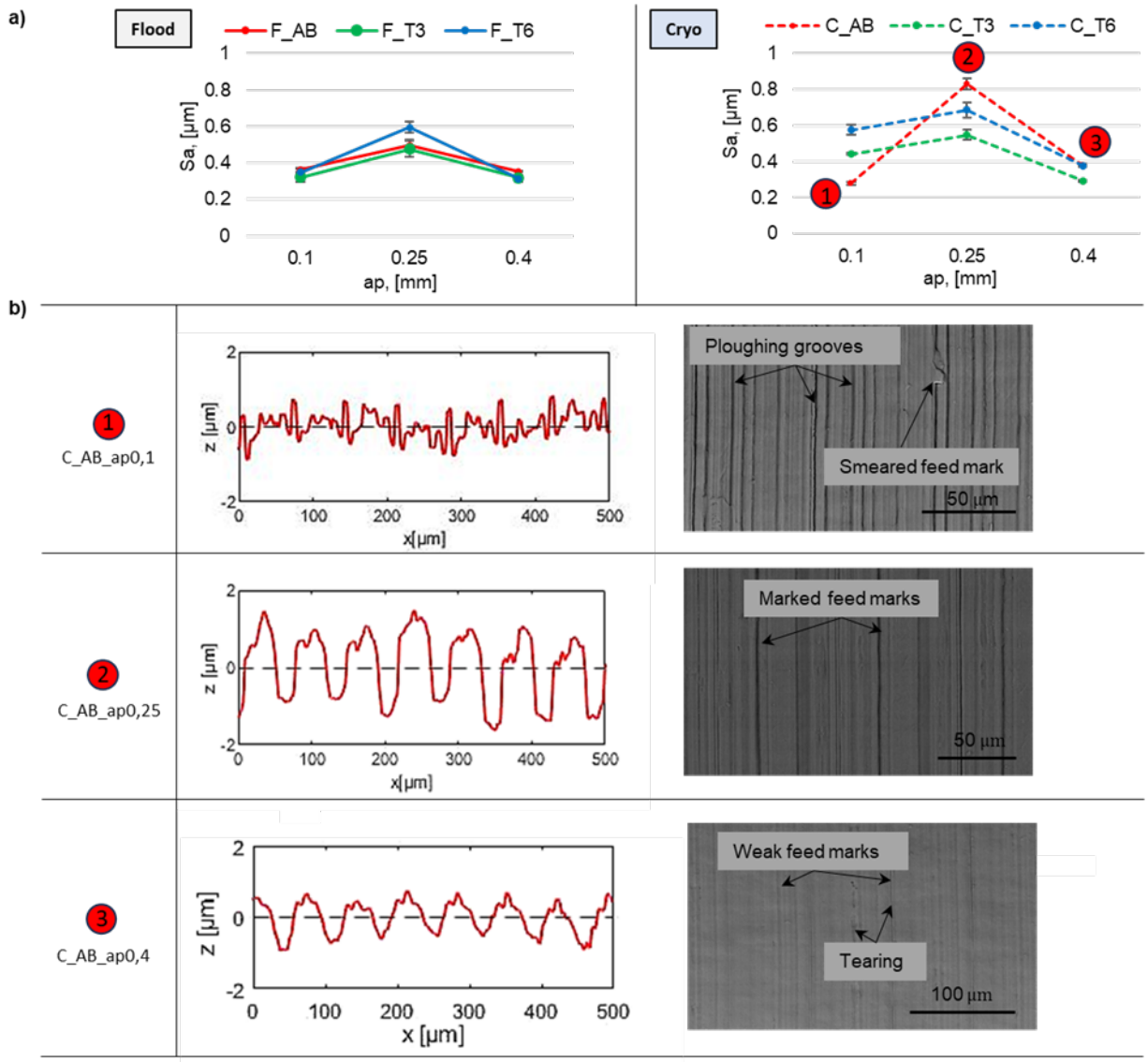

Fig. 3: a) Surface roughness of the AB, T3, and T6 flood and cryogenic machined samples at varying depth of cut, b) roughness profile and surface appearance of the AB samples cryogenic machined at varying depth of cut.

Therefore, the significant difference in surface finish found in case of cryogenic machining can be attributed to the varying thermal conditions that the material undergoes during the machining itself

Fig. 3b shows the roughness profiles of the AB samples machined under cryogenic cooling, here reported as they show the greatest variation in terms of S_a at varying a_p, nevertheless the same trend was found in the other samples. The profiles are flanked by backscattered electron detector (BSED) images showing the characteristics and possible defects of the machined surfaces. The difference between the three roughness profiles is evident and support the following considerations: the profile obtained with a_p of 0.1 mm is the most irregular and it is difficult to detect the typical periodicity of the machined profile, even if it allows a low S_a. On the other hand, periodicity is present in the profiles obtained at intermediate (0.25 mm) and higher (0.4 mm) depths of cut, which is also confirmed by the fact that the distance between two successive peaks is 70 μm, corresponding to a feed of 0.07 mm/rev. However, at a_p of 0.25 mm the distance between

peaks and valleys is more pronounced than in the profile with a_p of 0.4 mm, thus demonstrating the higher S_a of the former compared to the latter.

The morphology of the machined surfaces can be better understood by looking at the corresponding BSED images. In the profile obtained with the lowest depth of cut, it is difficult to distinguish the feed marks that define the tool pass from the other grooves, which explains why the periodicity of the profile is almost lost. It is therefore observed that the surface machined at $a_p$of 0.1 mm is affected by ploughing grooves. Although the depth of cut of 0.1 mm is within the range allowed by the tool manufacturer for the adopted cutting tool, the appearance of ploughing grooves is well associated with using a depth of cut equal to the radius of the tool nose. Consequently, this phenomenon influences the components of the machining force, with the radial component surpassing the feed force, thereby impacting the surface finish of the workpiece.

In the profiles where the peaks and valleys are more pronounced, the different tool passes are clearly distinguishable by the presence of visible feed marks. This last aspect is particularly noticeable with a_p of 0.25 mm, which also has the worst S_a values. In the profile with the highest depth of cut, the surface roughness decreases. In fact, the distance between the valleys and peaks decreases and, consequently, the feed marks become less pronounced, and it can be also observed that the machined surface is subjected to tearing and ripping.

To enhance the comprehension of the morphology of the machined surfaces, SEM observations were conducted with the BSED detector to analyze the insert state after machining. It must be underlined that each turning operation was carried out making use of a virgin insert, therefore the wear observed on the insert is specific to that operation. Fig. 4 displays the SEM images of the flank of the inserts used to machine the T3 samples under cryogenic cooling conditions at varying depth of cut, nevertheless the tool state when machining the AB and T6 samples was the same, and therefore not here displayed. As expected from the analysis of the roughness profiles, the least worn tool is the one that worked at a_p of 0.1 mm. The wear was limited to the cutting-edge area since, as mentioned earlier, the depth of cut corresponds to the radius of the tool nose. The tool's condition worsens at a_p of 0.25 mm and there are also visible traces of material adhering to the workpiece. At a_p of 0.4 mm, the built-up edge (BUE) and built-up layer (BUL) phenomena become even more noticeable. The first case refers to when the material adheres to the tool in the cutting zone, while in the latter case, the material adheres to the rake face of the tool. The tool geometry is altered by the presence of BUE and BUL, resulting in a better surface finish leading to a decrease in roughness, as reported in [12].

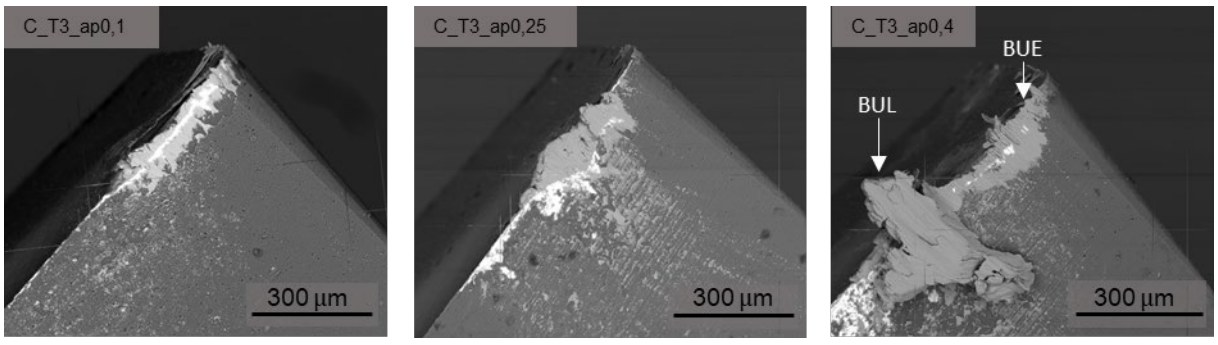

Fig. 4: State of the tool flank faces when cryogenic machining T3 samples at varying depth of cut.

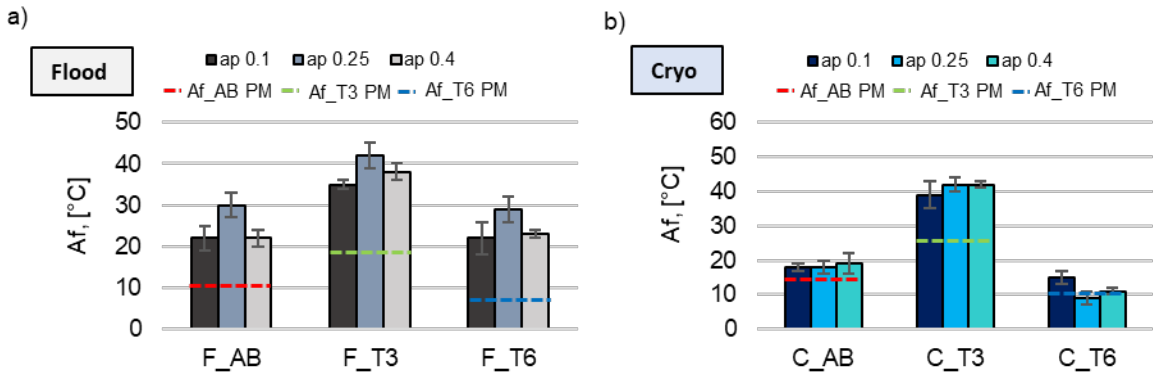

Fig. 5: Austenite finish temperature of the AB, T3, and T6 samples machined at different depths of cut under a) flood and b) cryogenic cooling conditions.

Fig. 5 displays the austenite finish temperature (A_f) values, which determine whether the sample is in the austenitic phase at room temperature, i.e. when A_f is approximately below 24°C. Fig. 5 shows that machining always increases A_f and only in the cases of the cryogenically machined AB and T6 samples the material can be considered still austenitic at room temperature. On the contrary, flood machining resulted in non-austenitic samples at room temperature, regardless of the depth of cut and sample microstructure. This issue was also observed in the case of T3 samples that were cryogenically machined.
On the other hand, the samples before machining were all austenitic at 24°C, as shown by the dotted lines in the histograms of Fig. 5.

When coming to the influence of the depth of cut, the highest increase in A_f was obtained at a_p of 0.25 mm in the flood conditions, regardless of the material microstructure. It is worth noting that the same trend observed for the surface roughness at varying depth of cut was found for A_f in case of flood machining. On the other hand, in case of cryogenic machined samples, the influence of the depth of cut in varying A_f can be considered negligible, as a consequence of the cutting temperature reduction that limits any effect on the NiTi microstructure, and thus transformation temperatures. The material microstructure is still the parameter most influencing the A_f values also after machining. On the contrary, the effect of the depth of cut is more marginally evident.

Conclusions

This study evaluates the effect of the process parameters on Ni-rich NiTi samples obtained by AM and subjected to heat treatment and finishing machining. Based on the results discussed so far, the following conclusions can be drawn:

- The microstructure is clearly different between the as-built (AB), 300°C-aged (T3) and 600°C-aged (T6) NiTi samples. Additionally, the calorimetric analysis indicates that the T3 sample has the highest austenite finish temperature, followed by the AB sample and finally the T6 one.
- Cryogenic machining produced more differentiated surface roughness results when varying the depth of cut. This behaviour can be attributed to the material phase change that can occur during cryogenic machining. In fact, at $a_p$of 0.25 mm, the alloy is presumed to be martensitic, while at $a_p$of 0.4 mm, it has reverted to the austenitic or quasi-austenitic phase as the temperature increases due to a greater depth of cut. Finish machining typically results in an increase in transformation temperatures, but this effect is less pronounced when cryogenic processing.
- The depth of cut of 0.25 mm yields the highest values of S_a, regardless of the sample's microstructure or the machining condition adopted. In fact, the roughness profiles show that a_p of 0.25 mm leads to a greater distance between the peaks and valleys compared to the other

profiles. Observations were made regarding the surface and tool conditions used for each depth of cut. The insert that worked at a_p of 0.4 mm produced a better surface finish than the one that worked at a_p of 0.25 mm. Regarding the austenite finish temperature, it appears that the 0.25 mm depth of cut resulted in a greater increase in A_f. However, this trend was only observed in the flood machining case.

Acknowledgments
This research was developed in the framework of the PRIN project "NEMESI - 4D manufacturing based on 3D printing and machining for Nitinol biomedical and sensing applications" funded by the Italian Ministry of University and Research (MUR).

References

[1] G.B. Kauffman., M. Isaac, The story of nitinol: the serendipitous discovery of the memory metal and its applications, The chemical educator 2 (1997): 1-21. https://doi.org/10.1007/s00897970111a

[2] E. Patoor, D.C. Lagoudas, P.B. Entchev, L.C. Brinson, X. Gao, Shape memory alloys, Part I: General properties and modeling of single crystals, Mechanics of materials, 38.5-6 (2006), 391-429. https://doi.org/10.1016/j.mechmat.2005.05.027

[3] M. Elahinia, N. Shayesteh Moghaddam, M. Taheri Andani, A. Amerinatanzi, B. A. Bimber, R. F. Hamilton, Fabrication of NiTi through additive manufacturing: A review, Progress in Materials Science, vol. 83. Elsevier Ltd, pp. 630–663, Oct. 01, 2016. https://doi.org/10.1016/j.pmatsci.2016.08.001

[4] Y. Kaynak, H. E. Karaca, I. S. Jawahir, Cutting speed dependent microstructure and transformation behavior of NiTi alloy in dry and cryogenic machining, Journal of Materials Engineering and Performance 24 (2015): 452-460. https://doi.org/10.1007/s11665-014-1247-6

[5] H. Yang, K. Sakai, H. Shizuka, Y. Kurebayashi, K. Hayakawa, T. Nagare, Effect of cutting speed on shape recovery of work material in cutting process of super-elastic NiTi alloy, International Journal of Automation Technology, 15.1 (2021), 24-33. https://doi.org/10.20965/ijat.2021.p0024

[6] R. Bertolini, S. Bruschi, A. Ghiotti, E. Savio, L. Ceseracciu, I.S. Jawahir, Surface integrity and superelastic response of additively manufactured Nitinol after heat treatment and finish machining, CIRP Annals (2023). https://doi.org/10.1016/j.cirp.2023.04.025

[7] S. Khademzadeh, F. Zanini, J. Rocco, K. Brunelli, P.F. Bariani, S. Carmignato, Quality enhancement of microstructure and surface topography of NiTi parts produced by laser powder bed fusion, CIRP Journal of Manufacturing Science and Technology 31 (2020), 575-582. https://doi.org/10.1016/j.cirp.2023.04.025

[8] A. Bordin, S. Bruschi, A. Ghiotti, P.F. Bariani, Analysis of tool wear in cryogenic machining of additive manufactured Ti6Al4V alloy, Wear 328 (2015), 89-99. https://doi.org/10.1016/j.wear.2015.01.030

[9] ASTM F2004-17: Standard Test Method for Transformation Temperature of Nickel-Titanium Alloys by Thermal Analysis.

[10] BS EN ISO 25178-2:2022: Geometrical product specifications (GPS). Surface texture: Areal. Terms, definitions and surface texture parameters.

[11] X. B Wang, B. Verlinden, J. Van Humbeeck, R-phase transformation in NiTi alloys, Materials Science and Technology (United Kingdom), vol. 30, no. 13, pp. 1517–1529 (2014). https://doi.org/10.1179/1743284714Y.0000000590

[12] R. Bertolini, A. Ghiotti, S. Bruschi, Graphene nanoplatelets as additives to MQL for improving tool life in machining Inconel 718 alloy, Wear 476 (2021), 203656. https://doi.org/10.1016/j.wear.2021.203656